

# Chimera states in population dynamics: networks with fragmented and hierarchical connectivities

Johanne Hizanidis,<sup>1,2,\*</sup> Evangelia Panagakou,<sup>1</sup> Iryna Omelchenko,<sup>3</sup>  
Eckehard Schöll,<sup>3</sup> Philipp Hövel,<sup>3,4</sup> and Astero Provata<sup>1</sup>

<sup>1</sup>*Institute of Nanoscience and Nanotechnology, National Center for Scientific Research “Demokritos”, 15310 Athens, Greece*

<sup>2</sup>*Crete Center for Quantum Complexity and Nanotechnology,*

*Department of Physics, University of Crete, 71003 Heraklion, Greece*

<sup>3</sup>*Institut für Theoretische Physik, Technische Universität Berlin, Hardenbergstraße 36, 10623 Berlin, Germany*

<sup>4</sup>*Bernstein Center for Computational Neuroscience Berlin,*

*Humboldt-Universität zu Berlin, Philippstraße 13, 10115 Berlin, Germany*

(Dated: May 1, 2015)

We study numerically the development of chimera states in networks of nonlocally coupled oscillators whose limit cycles emerge from a Hopf bifurcation. This dynamical system is inspired from population dynamics and consists of three interacting species in cyclic reactions. The complexity of the dynamics arises from the presence of a limit cycle and four fixed points. When the bifurcation parameter increases away from the Hopf bifurcation the trajectory approaches the heteroclinic invariant manifolds of the fixed points producing spikes, followed by long resting periods. We observe chimera states in this spiking regime as a coexistence of coherence (synchronization) and incoherence (desynchronization) in a one-dimensional ring with nonlocal coupling, and demonstrate that their multiplicity depends both on the system and the coupling parameters. We also show that hierarchical (fractal) coupling topologies induce traveling multichimera states. The speed of motion of the coherent and incoherent parts along the ring is computed through the Fourier spectra of the corresponding dynamics.

PACS numbers: 89.75.Fb; 05.45.Df; 05.45.Ra; 05.45.Xt; 05.45.-a

Keywords: Chimera state, lattice limit cycle model, Hopf bifurcation, networks, connectivity matrix, hierarchical connectivity.

## I. INTRODUCTION

The recent influence of the theory of networks [1–3] on the classic field of coupled oscillatory units [4] has led to the discovery of a plethora of novel phenomena, especially when the coupling between units becomes more sophisticated, mimicking naturally interacting systems. Among the complex oscillatory patterns that may emerge, are the so-called “chimera states” [5, 6], which have recently attracted a lot of attention. These are states, in which identically coupled units spontaneously develop coexisting synchronous (coherent) and asynchronous (incoherent) parts.

Many recent theoretical works have focused on the study of chimera states in a variety of physical systems. Typical models that have been numerically investigated include the Kuramoto phase oscillator [7–9], periodic and chaotic maps [10, 11], the Stuart-Landau model [13, 14], the Van der Pol oscillator [12] as well as models addressing neuron dynamics such the FitzHugh-Nagumo oscillator [15], the Hindmarsh-Rose model [16], the so-called SNIPER model of excitability type-I [17], or the Hodgkin-Huxley model [18]. Moreover, chimera states have been reported in populations of coupled pendula [19], in autonomous Boolean networks [20], in one-

dimensional superconducting meta-materials [21], and time-varying networks [22].

Following the theoretical predictions, chimera states were experimentally verified for the first time in populations of coupled chemical oscillators [23] and in optical coupled-map lattices realized by liquid-crystal light modulators [24]. Recently, in a purely mechanical experiment involving two groups of identical metronomes, it was shown that chimeras emerge naturally as a coexistence of two competing synchronization patterns [25]. Chimeras were also realized in experiments involving electronic nonlinear oscillators with delay [26] and electrochemical oscillator systems [27, 28].

Chimera states find increasing interest due to the possible connections to various phenomena observed in biological and social systems. As stated in the review paper of Panaggio and Abrams [29], chimera states could possibly explain the phenomenon of unihemispheric sleep observed in dolphins and some birds which sleep with half of their brain [30] as well as ventricular fibrillation [31].

In the current study, we attempt to bring in evidence chimera states in the fields of chemical reaction kinetics and ecology. Ecological models in the form of reactive dynamical systems have been previously used to describe the interactions between multiple species (referred to also as particles). In most cases the dynamics follows a mean field (MF) rate equations approach, which describe global dynamical features [32, 33]. In addition, numerical simulations are employed to address specific details of the

---

\*corresponding author: hizanidis@physics.uoc.gr

spatial and temporal characteristics of the systems [34–36]. Along the same lines, dynamical systems describing interactions between different chemical species are studied. Common examples involving heterogeneous catalytic dynamics are the reactions  $NO + CO$  [37, 38],  $CO + O_2$  [38, 39],  $CO + OH$  [40], all taking place on a platinum catalyst, the reaction  $CO + 2H_2$  on various catalysts [41], etc. All above processes are described as dynamical systems using the Langmuir-Hinshelwood mechanism [42]. Analogous modeling is extensively used for the well known oscillatory Belousov-Zhabotinsky reaction [43, 44]. In epidemiology, reactive systems are frequently used where the species correspond to infected individuals, susceptible or recovered ones, and they can dynamically infect other parts of the population [45–47]. All these systems are commonly viewed as reactive dynamics involving reaction, birth (or adsorption), and death (desorption) processes.

In the field of experimental reactive dynamics there have already been several studies discussing the existence of chimera states. Some interesting works include the photosensitive Belousov-Zhabotinsky reaction [23] as well as experiments with electrochemical oscillators [27, 28]. Similarly, a social analogue of a chimera state was reported in [49], where the authors investigated the emergence of localized coherence in two interacting populations of social agents. Two social models were implemented, the Axelrod model for culture dissemination [50] and the bounded confidence model by Deffuant et al. [51]. Different synchronization patterns were obtained, including chimera states where one subpopulation of agents remained synchronized while the other was desynchronized.

It is interesting to note here that in all experiments as well as in the social systems presented above, the subpopulations of elements are *ab initio* prepared and serve as a basis for the synchronized/desynchronized activity. On the other hand, in the numerical investigations cited above and in the current study, the coherent/incoherent regions emerge spontaneously from the interplay between the system parameters, dynamics, and initial conditions.

The main ingredients for the emergence of a chimera state in coupled oscillatory dynamics is the stable oscillatory pattern of the single elements together with the nonlocal character of the interactions. A toy model which exhibits well defined oscillations in the form of a limit cycle and is relevant in ecological, chemical, and social dynamics is the Lattice Limit Cycle (LLC) model, proposed in [48]. The LLC model is a nonlinear system that describes reaction, birth, and death processes and studies how the concentrations of the specific species change with time under the influence of the control parameters. The LLC is an ideal model to study the development of chimera states in population dynamics for three reasons: (a) It describes common ecological/social/chemical processes using reaction, birth, and death differential equations, (b) its dynamics is characterized by a limit cycle, and (c) when needed, it allows for direct implementa-

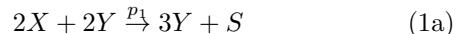
tion on a lattice with single species occupancy for a more realistic representation of the dynamics.

In this study, the capacity of the LLC model to produce chimera states will be investigated. The chimera attributes will be discussed as the system approaches the critical point of the Hopf bifurcation. Furthermore, we will explore the influence of the connection topology on the chimera features. In population dynamics, exchange in the form of spatial diffusion between individuals residing on different parts of the system is frequent: people move from one city to another, birds migrate, individual animals circulate from one herd to another, etc. In natural and social dynamics, the circulation of individuals has often nonlocal character and thus it is natural to investigate phenomena like chimera states which have their origin in nonlocal interactions. In particular, it is important to consider hierarchical connectivity in the coupling of the LLC dynamics, since the habitats of populations have often hierarchical/fractal distributions and morphologies: the city locations are fractally distributed [52], the mammal and bird habitats are located on fragmented landscapes that affect their community dynamics [53–55], and the viruses spread in complex socio-geographic networks [56, 57]. As we will see in the sequel, hierarchical connectivity induces traveling chimera states, a novel feature in this field.

The work is organized as follows: In Sec. II we recapitulate the main properties of the the LLC model, the MF approach, its temporal behaviour and bifurcation scenario. In Sec. III we define the system’s spatial geometry on a ring with classical nonlocal coupling and we numerically demonstrate the emergence of chimera states in dependence of the coupling range and the distance from the critical point. In Sec. IV we introduce fractal connectivity matrices and give evidence of traveling chimeras. Additional results on connectivity with gaps are included in the Appendix. In the concluding section we summarize our results and discuss open problems.

## II. PARAMETRIC STUDY OF THE LATTICE LIMIT CYCLE MODEL

Originally, the LLC scheme [48] was devised as a highly nonlinear model for a cyclic reaction-diffusion process with predator-prey interactions among three particles  $X$ ,  $Y$ , and  $S$ . The reaction scheme reads:



where  $p_1$ ,  $p_2$ , and  $p_3$  are the interaction rates.

The system (1) being an ecological model was inspired by heterogeneous catalytic reactions, where single particles are deposited on the sites of a catalyst surface. These particles interact with their neighbors or diffuse on the

surface. The catalyst is usually represented as a regular two-dimensional (2D) lattice (square, honeycomb, triangular), or even as a fractal lattice with impurities [58]. These catalytic applications indicate the need to represent the empty lattice sites as a virtual species, which participates in the reaction and diffusion processes as well. The LLC model thus involves one virtual species,  $S$ , which represents the empty sites and two “normal” species,  $X$  and  $Y$ , which are engaged in the three reactions. The scheme (1) describes that the interaction of two particles  $X$  and two particles  $Y$  turns one of the  $X$ -particles into  $Y$  while the other  $X$ -particle turns into  $S$  [Eq. (1a)]. The positions (lattice sites) where the particles are located may or may not be first neighbors, depending on the model (see Ref. [59]). Similarly, Eq. (1b) represents the birth of  $X$  if another  $X$  is found in an adjacent position, while Eq. (1c) represents the cooperative death of a particle  $Y$  leaving an empty site  $S$ .

This model has been extensively studied in recent years. Initially, it was implemented on a square lattice with single occupancy per lattice site using Kinetic Monte Carlo (KMC) simulations. Direct KMC realizations on the 2D square lattice with nearest neighbor inter-

actions produced intricate fractal patterns and local oscillations of the species concentrations [48]. Later on, long-distance diffusion was introduced as a mixing mechanism allowing the species to react with all particles within a specific range, thus giving them the possibility to change their places in the lattice at finite or infinite distances [59]. The model was also studied from the viewpoint of an abstract network of phases that was shown to have features of a scale-free network through calculations of the degree distribution and clustering coefficient [60].

In the MF approach, the system is described by three 4th-order nonlinear differential equations for the temporal total concentrations  $x$ ,  $y$ , and  $s$  of the respective particles  $X$ ,  $Y$ , and  $S$ . After applying the conservation condition  $x + y + s = 1$ , the LLC system is reduced to the following two equations:

$$\frac{dx}{dt} = -2p_1x^2y^2 + p_2x(1 - x - y) \quad (2a)$$

$$\frac{dy}{dt} = p_1x^2y^2 - p_3y(1 - x - y). \quad (2b)$$

The LLC system (Eq. (2)) has four fixed points: one saddle-point  $Q_1 = (0, 0)$ , two other fixed points  $Q_2 = (0, 1)$  with an unstable eigenvector direction along the  $y$ -axis and  $Q_3 = (1, 0)$  with a stable eigenvector direction along the  $x$ -axis (each having one zero eigenvalue [48]), and one nontrivial fixed point whose coordinates depend on the system parameters:  $Q_4 = \left( \sqrt[3]{\frac{p_3^2}{p_1p_2} [1 + K]} + \sqrt[3]{\frac{p_3^2}{p_1p_2} [1 - K]}, \sqrt[3]{\frac{p_2^2}{8p_1p_3} [1 + K]} + \sqrt[3]{\frac{p_2^2}{8p_1p_3} [1 - K]} \right)$  with  $K = \sqrt{\frac{1 + (2p_3 + p_2)^3}{27p_1p_2p_3}}$ . In the parameter space  $(p_1, p_2)$  for fixed  $p_3$ ,  $Q_4$  is either a stable node or a stable focus which becomes unstable through a supercritical Hopf bifurcation [48]. Because of the physical condition  $x, y, s \geq 0$  the flow is always directed to the inside of the reaction simplex  $x > 0, y > 0, x + y < 1$  which follows from mass-action kinetics.

Hereafter, we fix the parameters  $p_2 = 0.5$  and  $p_3 = 0.8$ , while  $p_1$  will be used as a control parameter determining the distance from the bifurcation point. For the above values of  $p_2$  and  $p_3$ , it can be found that the Hopf bifurcation takes place at  $p_1^{crit} = 9.82$ . Figure 1(a) shows the limit cycle for three different values of  $p_1 > p_1^{crit}$ , while the amplitude and period of the limit cycle as a function of  $p_1$  is plotted in Figs. 1(b) and (c), respectively. The  $x$  and  $y$  time series corresponding to the limit cycles of Fig. 1(a) are depicted in Figs. 1(d) and (e), respectively. In the time series of the  $y$ -variable, in particular, the sharp spikes followed by long resting periods are visible for large values of  $p_1$ .

In the current study, we consider a setup based on MF oscillators arranged on a cyclic one-dimensional network (ring), interacting linearly with one another. The use of the MF dynamics on all network sites mimics the interactions between populations, where each population is composed of a mixture of  $x$ ,  $y$ , and  $s$ . While the nodes interact with one another via nonlocal coupling as will be explained in the next section, the resident population follows the MF approach on each node given by Eqs. (2). This is a different approach than the previous KMC simu-

lations [36, 48], where each node (lattice site) is occupied by a single particle. The properties of this particular arrangement of the populations is discussed in detail in the following section.

### III. MULTICHIMERA STATES IN THE LATTICE LIMIT CYCLE MODEL

We consider  $N$  nonlocally coupled LLC oscillators on a one-dimensional ring according to the following scheme:

$$\frac{dx_k}{dt} = -2p_1x_k^2y_k^2 + p_2x_k(1 - x_k - y_k) + \frac{\sigma}{2R} \sum_{j=k-R}^{j=k+R} (x_j - x_k) \quad (3a)$$

$$\frac{dy_k}{dt} = p_1x_k^2y_k^2 - p_3y_k(1 - x_k - y_k) + \frac{\sigma}{2R} \sum_{j=k-R}^{j=k+R} (y_j - y_k), \quad (3b)$$

where the subscript  $k$  refers to the node index,  $k = 1, \dots, N$ , which has to be taken modulo  $N$ . Each os-

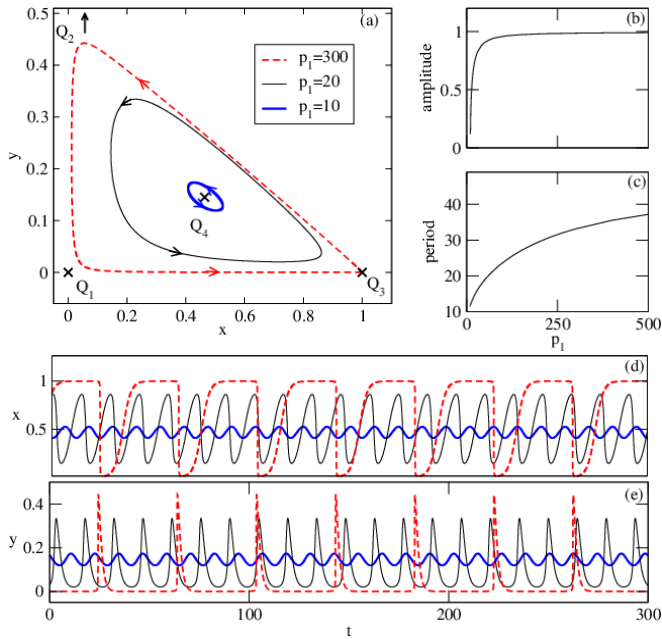


Figure 1: (Color online) (a) Limit cycle for various values of  $p_1$  above the Hopf bifurcation. Fixed points  $Q_1, Q_2$  (not shown),  $Q_3$ , and  $Q_4$  (for  $p_1 = 10$ ) are marked with crosses. (b) Peak-to-peak amplitude of the  $x$ -variable and (c) Period of the limit cycle as a function of  $p_1$ . (d) and (e) show the time series of  $x$  and  $y$ , respectively, corresponding to the limit cycles in (a). Other parameters:  $p_2 = 0.5$  and  $p_3 = 0.8$ .

cillator is coupled with its  $R > 0$  nearest neighbors on both sides with coupling strength  $\sigma$ . This introduces nonlocality in the form of a ring topology as proposed in Ref. [15, 61]. There, the authors considered a rotational coupling matrix in order to achieve both direct and cross-coupling between the system variables. Our system is simpler in the sense that it contains only direct coupling in the species concentrations. This reflects mobility of the species between nodes and no cross-interactions of species between different nodes.

A typical chimera state with two (in)coherent regions is shown in Fig. 2(a), where the  $x$ -concentration is plotted as snapshot. Initial conditions in all simulations herein are taken to be randomly distributed on an ellipsoid enclosed by the triangle with corners on the fixed points  $Q_1, Q_2$ , and  $Q_3$ . As a measure indicating the existence of a chimera state we employ the *mean phase velocity* of each oscillator  $\omega_k = 2\pi M_k / \Delta T$ , where  $M_k$  is the number of periods of the  $k$ th oscillator during a time interval  $\Delta T$  [5, 15]. This quantity is depicted in Fig. 2(b) and has the typical profile: flat, lower-valued in the coherent domains and arc-shaped, higher-valued, in the incoherent ones. Figure 2(c) shows a snapshot of the  $(x, y)$ -plane (red dots) together with the limit cycle of the uncoupled system for the same parameter values. We observe that the coupling results in a limit cycle with smaller amplitude than in the corresponding uncoupled system. Finally, in the space-time plot of the  $x$  variable in Fig. 2(d),

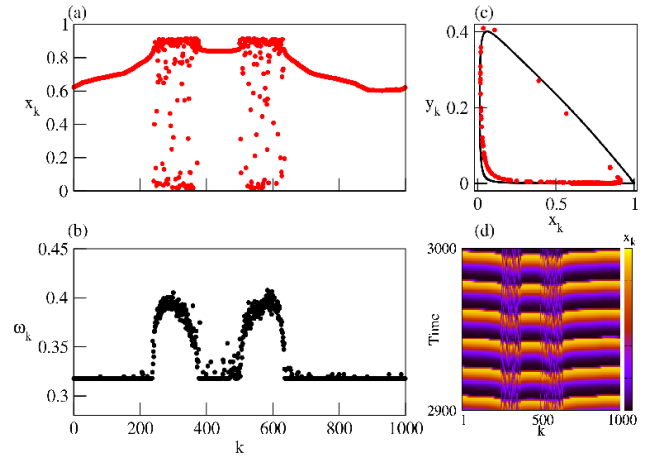


Figure 2: (Color online) (a) Snapshot of the variable  $x_k$  of Eqs. (3) and (b) corresponding mean phase velocity profile. (c) Limit cycle of the uncoupled system (black solid line) and snapshot in the  $(x, y)$ -plane (red dots). (d) Space-time plot of variable  $x_k$ . Parameters:  $p_1 = 300$ ,  $p_2 = 0.5$ ,  $p_3 = 0.8$ ,  $N = 1000$ ,  $R = 350$ , and  $\sigma = 0.015$ .

it can be seen that the chimera state is fixed in space and has a period of approximately 18 time units, which corresponds to the period of the uncoupled system for a much lower value of  $p_1 \approx 40$ .

The presence of chimera states in ecological and population systems can account for different dynamical states in different nodes of the interacting systems. For example, in population dynamics where communities exchange individuals, the density of inhabitants in some communities may oscillate in phase, while in other communities it may be incoherent. Similarly, in computer networks, the density of users (or the data exchange) may oscillate coherently in some parts of the network, while in other parts it may behave asynchronously.

In the following, we discuss how the coupling range  $R$  and the distance from the Hopf bifurcation, expressed through parameter  $p_1$ , influence the form and multiplicity of chimera states.

### A. Impact of coupling range $R$

Chimera states with multiple domains of incoherence and coherence have been reported in several works and are referred to as clustered chimera or multichimera states. It is known that they may be achieved through time delay [62] or by manipulating the range of the coupling between oscillators [15–17, 63]. The range  $R$  of the coupling reflects the migration range of the different species in the system. Therefore, it is interesting to verify the formation of clustered chimera states in our system by varying this quantity.

Figure 3 shows typical chimera states and correspond-

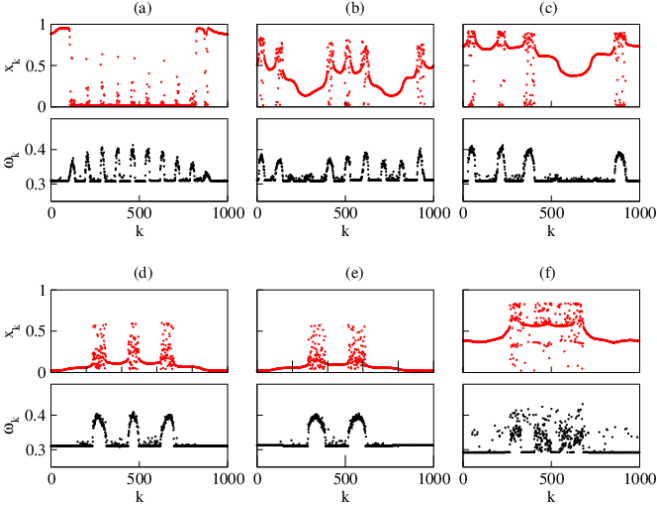


Figure 3: (Color online) Snapshots of the  $x$ -variable (red dots) and corresponding  $\omega_k$  profiles (black dots) for various values of the coupling range: (a)  $R = 100$ , (b)  $R = 120$ , (c)  $R = 190$ , (d)  $R = 230$ , (e)  $R = 280$ , and (f)  $R = 410$ . Other parameters as in Fig. 2.

ing mean phase velocity profiles for increasing  $R$ . For low values of the coupling range, chimera states with up to 10 (in)coherent domains may be found [Fig. 3(a)]. For increasing  $R$  the multiplicity of the chimera state decreases and, as  $R$  approaches the value of 280, a chimera state with 2 (in)coherent domains is found [Fig. 3(e)]. This 2-chimera state persists over a large  $R$ -interval up to  $R \approx 400$ , where it starts to deform [Fig. 3(f)]. The corresponding mean phase velocity profiles follow the multiplicity of the chimera states, exhibiting maximum values in the incoherent domains and constant values in the coherent domains.

### B. Impact of bifurcation parameter $p_1$

As mentioned in the Introduction, for fixed rates  $p_2$  and  $p_3$ , a Hopf bifurcation occurs at  $p_1^c \approx 9.82$  and a limit cycle starting from zero amplitude and finite period is born [see Figs. 1(b) and (c)]. As  $p_1$  increases, the limit cycle approaches the heteroclinic invariant manifolds from  $Q_2$  to  $Q_1$  and from  $Q_1$  to  $Q_3$  which bound the basin of attraction of the limit cycle. The time to approach  $Q_3$  becomes very large, and accordingly, its period diverges as  $p_1$  increases further. Therefore,  $p_1$  is a crucial parameter that introduces two time-scales in the system dynamics and determines the period of the individual oscillators. Physically,  $p_1$  determines the rate of reactive process (1a) and introduces a 4th-order term in the equations, since it requires simultaneous interaction of four species (particles). This parameter takes high values compared to the other two,  $p_2$  and  $p_3$ , to compensate the contribution of the term  $x^2 y^2$ .

Figure 4 shows typical snapshots of the  $x$ -variable and

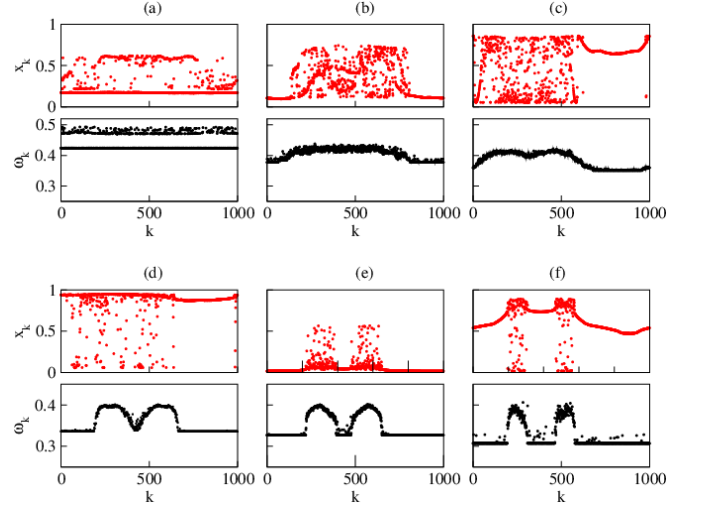


Figure 4: (Color online) Snapshots of the  $x$ -variable (red dots) and corresponding  $\omega_k$  profiles (black dots) at time  $t = 3000$ , for a fixed coupling range  $R = 350$  and various values of  $p_1$ : (a)  $p_1 = 20$ , (b)  $p_1 = 40$ , (c)  $p_1 = 90$ , (d)  $p_1 = 170$ , (e)  $p_1 = 210$  and (f)  $p_1 = 370$ . Other parameters as in Fig. 2.

corresponding mean phase velocity profiles for fixed coupling range  $R = 350$  and increasing  $p_1$ . For values of  $p_1$  close to the bifurcation point [Fig. 4(a)], no chimera state is observed but, instead, a mixed state with no obvious spatial structure is present where some oscillators cluster, while others move incoherently. This is also reflected in the mean phase velocity profile depicted in the lower panel of Fig. 4(a), which does not depict the characteristic arc of a chimera state. The amplitude of the oscillations for this parameter values is small. As we move away from the bifurcation point, the oscillators are organized in one coherent and one incoherent region, thus, forming a 1-chimera state [Figs. 4(b) and (c)]. The  $\omega_k$ -profile starts to obtain its typical shape, which becomes more prominent as  $p_1$  attains higher values. Then, a 2-chimera state appears around  $p_1 = 190$  [Figs. 4(e) and (f)].

A careful look at Figs. 4(c)-(f) reveals the scenario of how a chimera state with two incoherent parts is formed. The mean phase velocity profile develops a small dip, which increases and eventually reaches the level of the coherent part as the parameter  $p_1$  increases. Similar scenarios have been observed for nonlocally coupled FitzHugh-Nagumo systems [15].

The impact of  $p_1$  is also depicted in Fig. 5, where the space-time plots for the variable  $x$  (top panel) and the corresponding local order parameter (lower panel) are shown for fixed  $R = 350$ . The values of  $p_1$  are chosen as  $p_1 = 90, 170, 210$ , and  $370$  in panels 5(a) to 5(d), respectively, which corresponds to the snapshots in Figs. 4(c)-(f). The local order parameter is defined as follows [5, 64]:

$$Z_k = \left| \frac{1}{2\delta} \sum_{|j-k| \leq \delta} e^{i\Theta_j} \right|, \quad k = 1, \dots, N, \quad (4)$$

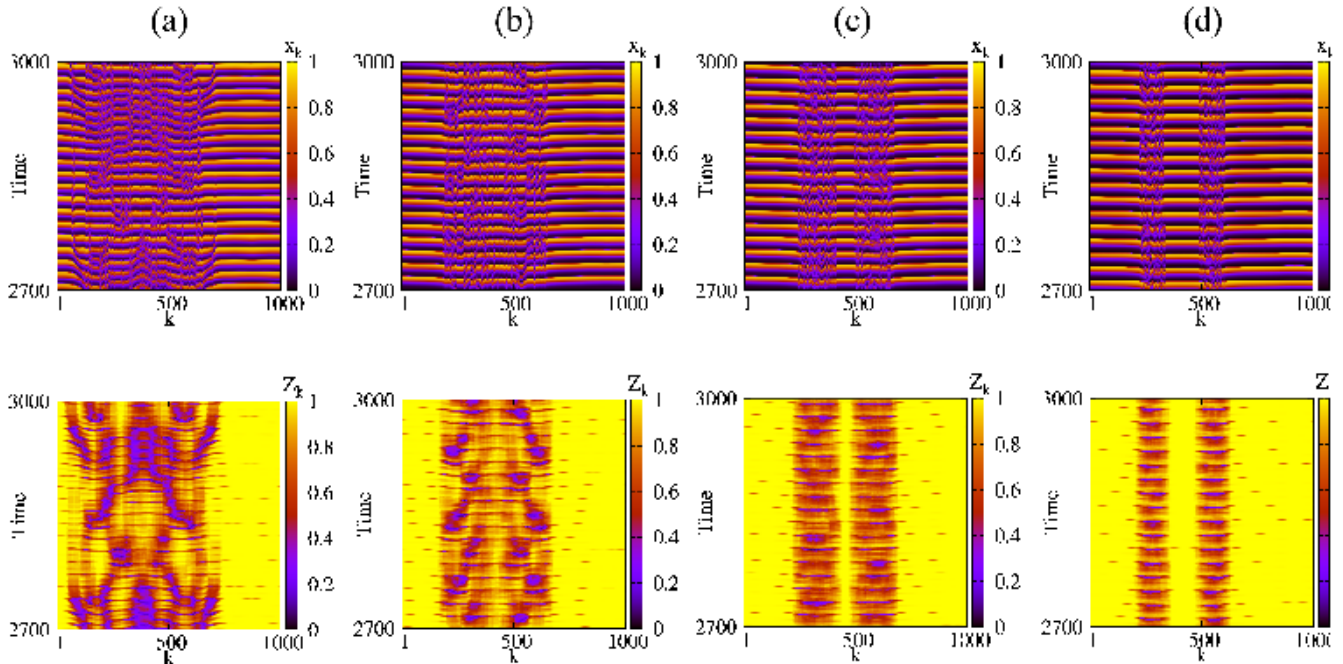


Figure 5: (Color online) Space-time plots of the  $x$ -variable (top) and order parameter (bottom) for fixed  $R = 350$  and increasing  $p_1$ : (a)  $p_1 = 90$ , (b)  $p_1 = 170$ , (c)  $p_1 = 210$ , and (d)  $p_1 = 370$ . Other parameters as in Fig. 2.

where  $\Theta_j = \arctan[(y_j - y_{Q_4})/(x_j - x_{Q_4})]$  denotes the geometric phase of the  $j$ th LLC unit and  $(x_{Q_4}, y_{Q_4})$  are the coordinates of the nontrivial fixed point  $Q_4$  of the uncoupled system. We use a spatial average with a window size of  $\delta = 25$  elements. The local order parameter  $Z_k$  close to unity indicates that the  $k$ th unit belongs to the coherent part of the chimera state, while  $Z_k$  is less than 1 for incoherent parts.

The lower panels of Fig. 5 depict the local order parameter in the time interval  $t \in [2700, 3000]$ , where bright (yellow) color denotes the coherent regions. A stationary 2-chimera state is obtained for high values of  $p_1$ , as shown in Fig. 5(d). As one moves closer to the Hopf bifurcation point, the two incoherent regions merge into a large one, while the size (number of oscillators) of the incoherent region increases at the expense of the coherent ones [Fig. 5(a) and (b)].

#### IV. TRAVELING CHIMERAS FOR HIERARCHICAL CONNECTIVITY

In a previous study on the FitzHugh-Nagumo model we have demonstrated that if the connectivity matrices have hierarchical form, the chimeras also occur as nested structures [64]. Here, in addition to these structures, we show evidence of a different phenomenon related to this connectivity, namely, the occurrence of traveling coherent/incoherent regions.

The hierarchical coupling structure involves connectivity gaps. The simplest example is a coupling matrix

with two gaps. The introduction of regular gaps induces merging and splitting of the (in)coherent parts of the chimera state but does not produce other qualitatively different features. Representative cases are shown in the Appendix A.

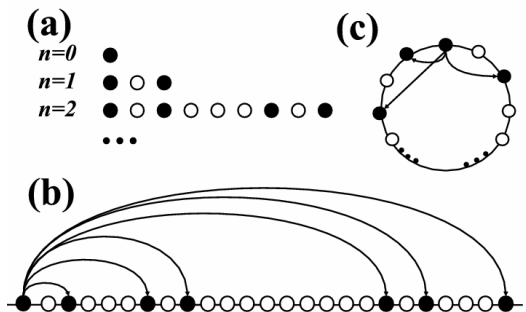


Figure 6: (Color online) Schematic representation of the hierarchical connectivity using the triadic Cantor set. (a) “bottom-up” construction of the triadic Cantor set, (b) linear connectivity arrangement and (c) ring connectivity arrangement for one reference node.

Before we discuss the effect of the hierarchical connectivity, we summarize the procedure to generate the corresponding network. Figure 6 illustrates this procedure in a schematic diagram [65]. Let us consider a connectivity matrix produced by an initiation string or base of size  $b$ , e.g.  $b = 3$  with a base pattern  $S = “101”$  in Fig. 6, con-



taining  $c_1$  times the symbol 1 and  $c_0 = b - c_1$  times the symbol 0. The specific arrangement of the symbols on the initiation string is essential, because the hierarchical connectivity pattern is constructed as the  $n$ th iteration of the initiation string replacing 1 by the base pattern  $S$  and 0 by  $b$  times the symbol 0. Thus, the length of the string defining the connectivity of the network is equal to the system size  $N = b^n$  and contains  $c_1^n$  times the symbol 1 and  $N - c_1^n$  the symbol 0. The limiting set, which is produced when the number of iterations  $n \rightarrow \infty$ , is a fractal Cantor set and has fractal dimension  $d_f = \ln c_1 / \ln b$ . Since  $d_f$  is formally defined for infinite systems only, the finite size sets used here are called hierarchical, because they have been constructed based on a hierarchical algorithm. As a last step, we obtain the total connectivity of the network by index shift. As we shift the iterated string along the ring, we can determine the connectivity for each node. In this construction, each node has precisely  $c_1^n$  links to other nodes hierarchically arranged in a unique pattern and directed. The corresponding connectivity matrix  $\{C_{kl}^{(n)}\}_{k,l=1,\dots,N}$  is given by

$$C_{kl}^{(n)} = \begin{cases} 1 & \text{if both nodes } k \text{ and } l \text{ belong to the} \\ & \text{Cantor set obtained by } n \text{ iterations} \\ 0 & \text{elsewhere.} \end{cases} \quad (5)$$

This connectivity matrix is of size  $b^n \times b^n$  and contains a hierarchical distribution of gaps with a variety of sizes.

In the following, we use the base size  $b = 6$  and  $n = 4$  iteration steps producing a system of size  $N = 6^4 = 1296$ . The considered initiation strings are  $S = \text{"001111"}$  and  $S = \text{"110111"}$ , which iterated  $n = 4$  times produce the connectivity patterns, consisting of 256 and 625 times the symbol 1 and 1040 and 671 times the symbol 0, respectively.

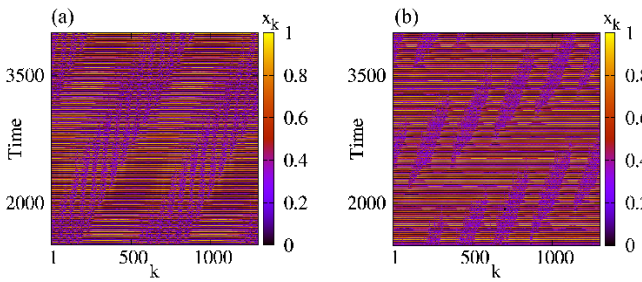


Figure 7: (Color online) Space-time plots of two traveling chimeras for (a)  $d_f = \ln 4 / \ln 6 = 0.774$  and initiation string “001111” and (b)  $d_f = \ln 5 / \ln 6 = 0.898$  and initiation string “110111”. All other parameters as in Fig. 2.

The motion of the (in)coherent regions in traveling chimeras are depicted in the space-time plots, Fig. 7(a) and (b). From this figure we can observe a continuous translation of the (in)coherent parts along the ring, a motion which is not observed, for example, in Fig. 5, where exemplary space-time plots of chimeras with fixed

position are presented. The space-time plots in Fig. 7 also reveal an additional internal nested structure in both cases which are the imprints of the hierarchical connectivity. Similar nested chimera states have been previously demonstrated by the FitzHugh-Nagumo system without the additional feature of traveling (in)coherent parts [64].

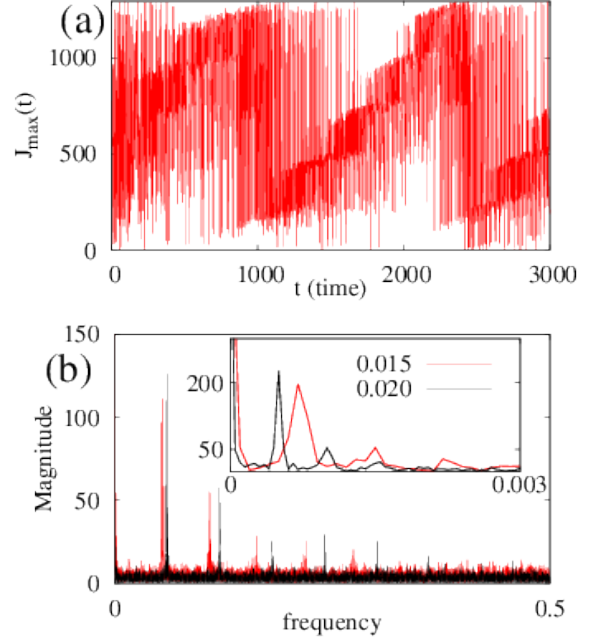


Figure 8: (Color online) (a) Position of the oscillator displaying maximum  $x$ -value with time for  $\sigma = 0.015$  and (b) Fourier transforms for  $\sigma = 0.015$  (red spectrum) and  $\sigma = 0.020$  (black spectrum). The inset in b) shows in detail the lowest part of the two spectra where the frequencies associated with the traveling motion around the ring are discerned. All other parameters as in Fig. 7(b).

In the case of traveling chimeras, the mean phase velocity is not a good measure for coherence, because each oscillator spends part of the time in the coherent regions and part of the time in the incoherent ones. An alternative way to distinguish between stationary and traveling chimeras is to locate the nodes attaining maximum and minimum  $x$ -values (or  $y$ -values) at each time step. Given that the incoherent regions are not localized but travel along the ring in time, we expect that the node (position on the ring) which achieves maximum  $x$ -values (or  $y$ -values) is also subject to change. In Fig. 8(a), we record the node,  $J_{\max}(t)$ , that exhibits maximum  $x$ -value at time  $t$ , which yields the condition:

$$x_{J_{\max}}(t) = \max \{x_1(t), x_2(t), \dots, x_N(t)\}. \quad (6)$$

Similarly, one can define the element  $J_{\min}(t)$ , which exhibits minimum value at time  $t$ . The position  $J_{\max}(t)$  (or  $J_{\min}(t)$ ) shows a periodicity, since each element successively passes through the state of maximum amplitude.

The period  $T$  needed for a single element to attain the state of maximum amplitude can be calculated using the Fourier transform of the time series  $J_{\max}(t)$ , Fig. 8(a). The Fourier transform, Fig. 8(b), presents two distinctive maxima. For example, for  $\sigma = 0.015$  we first observe in Fig. 8(b) (red line) one maximum of high frequency  $f_{\text{osc}} = 0.056$ , and short period  $T_{\text{osc}} = 1/f_{\text{osc}} = 17.86$  which correspond to the average frequency of the oscillators. By looking at the low frequencies (inset) we observe an additional maximum at frequency  $f_{\text{tr}} = 0.00071$  with long period  $T_{\text{tr}} = 1408$ , which is associated with the traveling motion around the ring. Note that  $T_{\text{osc}}$  is smaller than the period of the uncoupled oscillator  $T(p_1 = 300)$  [cf. Fig. 1(c)], because each unit is – from time to time – part of the incoherent domain, which oscillates faster than the coherent region. Furthermore, the traveling period  $T_{\text{tr}}$  can also be inferred from the time series  $J_{\max}$  shown in Fig. 8(a). The black curves in Figure 8(b) refer to a larger coupling strength  $\sigma = 0.02$  than the one used in all previous plots ( $\sigma = 0.015$ ). Comparing the spectra for the two  $\sigma$  values in Fig. 8(b) we find that the frequency  $f_{\text{tr}}$  moves to lower values as  $\sigma$  increases.

This is further detailed in Fig. 9 that shows the traveling speed  $v_{\text{tr}}$  of the domains. During one period  $T_{\text{tr}}$ , the coherent and incoherent regions cover the entire ring consisting of  $N$  elements, thus,

$$v_{\text{tr}} = N/T_{\text{tr}} = Nf_{\text{tr}} \quad (7)$$

The chimera traveling speed  $v_{\text{tr}}$  decreases for increasing coupling strength  $\sigma$ , i.e. as the coupling constant becomes larger, the incoherent regions slow down around the ring. We recall here the results of Sec. III where chimera states are only observed for low coupling strengths in the LLC model.

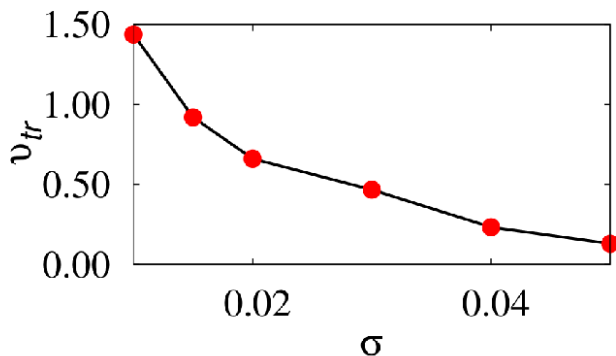


Figure 9: (Color online) Traveling speed  $v_{\text{tr}}$  of (in)coherent regions around the ring. All other parameters as in Fig. 7(b).

As alternative measure for the calculation of the traveling speed we may use the spectrum of single oscillators (not shown). Since each oscillator belongs periodically either to the coherent or the incoherent regions, it will participate once during each period in the regions which demonstrate maximum (or minimum) amplitude. Then

by calculating the spectrum of a single oscillator and selecting the lowest frequency we obtain an estimation of the chimera traveling speed  $v_{\text{tr}}$ , based on one oscillator. Average over the  $N$  elements needs to be taken to represent the overall chimera speed  $v_{\text{tr}}$ .

## V. CONCLUSIONS

In the present work, we have demonstrated for the first time the existence of chimera states in a population dynamics model, reflecting the various tendencies of local communities to behave (oscillate) coherently or incoherently within the same network. We have shown that the dynamics of the nonlocally coupled system strongly depends on the character of the local behavior of the nodes. When the parameters of the individual LLC nodes are close to the Hopf bifurcation, chimera states cannot be observed in the system. In this regime, all strongly nonlinear 4th-order terms become weak and the corresponding limit cycle oscillations lose their spiking form resembling simple harmonic motion of small amplitude. When the internal bifurcation parameter of each node increases away from the Hopf bifurcation, the trajectories approach the heteroclinic invariant manifolds of the saddle points producing spikes followed by long resting periods. This type of local dynamics allows for the existence of a variety of chimera and multichimera states, which depend both on the parameters of the individual system, and the coupling.

While the introduction of single gaps in the connectivity matrix induces merging and splitting of the (in)coherent parts of the chimera states (see Appendix A), hierarchical arrangement of gaps results in the emergence of nontrivial phenomena in which the (in)coherent regions show nested structures and travel along the ring, keeping their profiles statistically stable in time. Moreover, we have found that the speed of this motion decreases with increasing coupling strength. Complex nested chimera structures, when regarded from the viewpoint of population dynamics, show the rich organization which can emerge in communities of nonlinearly interacting populations.

## VI. ACKNOWLEDGMENTS

This work was supported by the German Academic Exchange Service (DAAD) and the Greek State Scholarship Foundation IKY within the PPP-IKYDA framework. JH and AP acknowledge support by YDISE project within GSRT's KRIPIS action, funded by Greece and the European Regional Development Fund of the European Union under NSRF 2007-2013 and the Regional Operational Program of Attica. PH acknowledge support by BMBF (grant no. 01Q1001B) in the framework of BCCN Berlin (Project A13). IO, ES, and PH acknowledge support by DFG in the framework of the Collaborative Re-



search Center 910. The research work was partially supported by the European Union's Seventh Framework Pro-

gram (FP7-REGPOT-2012-2013-1) under grant agreement n316165.

- 
- [1] D. J. Watts and S. H. Strogatz, *Nature* **393**, 440 (1998).
  - [2] E. Ravasz and A.-L. Barabási, *Phys. Rev. E* **67**, 026112 (2003).
  - [3] A.-L. Barabási, *Science* **325**, 412 (2009).
  - [4] V. S. Anishchenko, V. Astakhov, A. Neiman, T. Vadivasova, and L. Schimansky-Geier, *Nonlinear Dynamics of Chaotic and Stochastic Systems*, Springer-Verlang, Berlin 2007.
  - [5] Y. Kuramoto and D. Battogtokh, *Nonlinear Phenomena in Complex Systems* **5**, 380 (2002).
  - [6] D. M. Abrams and S. H. Strogatz, *Phys. Rev. Lett.* **93**, 174102 (2004).
  - [7] D. M. Abrams, R. Mirollo, S. H. Strogatz, and D. A. Willey, *Phys. Rev. Lett.* **101**, 084103 (2008).
  - [8] T. W. Ko and G. B. Ermentrout, *Phys. Rev. E* **78** 016203 (2008).
  - [9] C. R. Laing, K. Rajendran, and I. G. Kevrekidis, *Chaos* **22**, 013132, (2012).
  - [10] I. Omelchenko, Y. L. Maistrenko, P. Hövel, and E. Schöll, *Phys. Rev. Lett.* **106**, 234102 (2011).
  - [11] I. Omelchenko, B. Riemenschneider, P. Hövel, Y. Maistrenko, and E. Schöll, *Phys. Rev. E* **85**, 026212 (2012).
  - [12] I. Omelchenko, A. Zakharova, P. Hövel, J. Siebert, and E. Schöll, (2015) arXiv:1503.03377.
  - [13] C. R. Laing, *Phys. Rev. E* **81**, 066221 (2010).
  - [14] A. Zakharova, M. Kapeller, and E. Schöll, *Phys. Rev. Lett.* **112**, 154101 (2014).
  - [15] I. Omelchenko, O. Omel'chenko, P. Hövel, and E. Schöll, *Phys. Rev. Lett.* **110**, 224101 (2013).
  - [16] J. Hizanidis, V. Kanas, A. Bezerianos, and T. Bountis, *Int. J. of Bifurc. and Chaos* **24**, 1450030 (2013).
  - [17] A. Vüllings, J. Hizanidis, I. Omelchenko, and P. Hövel, *New J. Phys.* **16**, 123039 (2014).
  - [18] H. Sakaguchi, *Phys. Rev. E* **73**, 031907 (2006).
  - [19] T. Bountis, V. Kanas, J. Hizanidis, and A. Bezerianos, *Eur. Phys. J. Special Topic* **223**, 721 (2014).
  - [20] D. P. Rosin, D. Rontani, N. D. Haynes, E. Schöll, and D. J. Gauthier, *Phys. Rev. E* **90**, 030902(R) (2014).
  - [21] N. Lazarides, G. Neofotistos, and G. P. Tsironis, *Phys. Rev. B* **91**, 054303 (2015).
  - [22] A. Buscarino, M. Frasca, L. V. Gambuzza, and P. Hövel, *Phys. Rev. E* **91**, 022817 (2015).
  - [23] M. R. Tinsley and K. Showalter, *Nature Physics* **8**, 662 (2012).
  - [24] A. M. Hagerstrom, E. Thomas, R. Roy, P. Hövel, I. Omelchenko and E. Schöll, *Nature Physics* **8**, 658 (2012).
  - [25] E. A. Martens, S. Thutupalli, A. Fourrière, and O. Hallatschek, *Proc. Nat. Acad. Sciences* **110**, 10563 (2013).
  - [26] L. Larger, B. Penkovsky, and Y. L. Maistrenko, *Phys. Rev. Lett.* **111**, 054103 (2013).
  - [27] L. Schmidt, K. Schönleber, K. Krischer, and V. Garcia-Morales, *Chaos* **24** 013102 (2014).
  - [28] M. Wickramasinghe and I. Z. Kiss, *PLoS ONE* **8**, e80586 (2013).
  - [29] M. J. Panaggio and D. M. Abrams, *Nonlinearity* **28**, R67 (2015).
  - [30] R. Ma, J. Wang and Z. Liu, *Europhys. Lett.* **91**, 40006 (2010).
  - [31] J. M. Davidenko, A. V. Pertsov, R. Salomonsz, W. Baxter, and J. Jalife, *Nature* **355** (6358), 349 (1992).
  - [32] J. D. Murray, *Mathematical Biology*, Springer-Verlang, Berlin 1993.
  - [33] R. M. May, *Stability and Complexity in Model Ecosystems*, Princeton University Press, Princeton, 2001.
  - [34] A. Provata, G. Nicolis, and F. Baras, *J. Chem. Phys.* **110**, 8361 (1999).
  - [35] L. Frachebourg, P. L. Krapivsky, and E. Ben-Naim, *Phys. Rev. E* **54**, 6186 (1996).
  - [36] G. A. Tsekouras and A. Provata, *Phys. Rev. E* **65**, 056602 (2001).
  - [37] N. Khrustova, G. Veser, A. Mikhailov, and R. Imbihl, *Phys. Rev. Lett.* **75**, 3564 (1995).
  - [38] R. Imbihl and G. Ertl *Chem. Rev.* **95**, 697 (1995).
  - [39] V. K. Noussiou, and A. Provata, *Surface Science* **601**, 2941 (2007).
  - [40] A. B. Anderson and E. Grantscharova, *J. Phys. Chem.* **99**, 9149 (1995).
  - [41] N.S. Govender, F. G. Botes, M. H. J. M. de Croon, and J.C. Schouten, *J. Catalysis* **260**, 254 (2008).
  - [42] G. Ertl, *Surface Science* **299/300**, 742 (1994).
  - [43] I. R. Epstein and J. A. and Pojman, *An introduction to nonlinear chemical dynamics: oscillations, waves, patterns, and chaos*, Oxford University Press, New York, 1998.
  - [44] G. Nicolis and I. Prigogine, *Self-Organization in Nonequilibrium Systems*, Wiley, New York, 1977.
  - [45] R. M. Anderson and R. M. May, *Infectious Diseases of Humans*, Oxford University Press, Oxford, (1991).
  - [46] M. Delitala, *Math. and Comp. Modelling* **39**, 1 (2004).
  - [47] R. Pastor-Satorras and A. Vespignani, *Phys. Rev. Lett.* **86**, 3200 (2001).
  - [48] A. V. Shabunin, F. Baras. and A. Provata, *Phys. Rev. E* **66**, 036219 (2002).
  - [49] J. C. Gonzalez-Avella, M. G. Cosenza, and M. San Miguel, *Physica A* **399**, 24 (2014).
  - [50] R. Axelrod, *J. Conflict Res.* **41**, 203 (1997).
  - [51] G. Deffuant, D. Neau, F. Amblard, and G. Weisbuch, *Adv. Comp. Sys.* **3**, 87 (2000).
  - [52] M. Batty, *Science* **319**, 769 (2008).
  - [53] R. V. Solé, S.C. Manrubia, M. Benton, S. Kauffman, and B. Per, *Trends in Ecology and Evolution* **14**, 156 (1999).
  - [54] P. R. A. Campos, A. Rosas, V. M. de Oliveira, and M. A. F. Gomes *PLoS ONE* **8**, e66495 (2013).
  - [55] C. M. Buchmann, F. M. Schurr, R. Nathan, and F. Jeltsch, *Ecological Informatics* **14**, 90 (2013).
  - [56] R. Wallace, *Environment & Planning A* **26**, 767 (1994).
  - [57] M. Barthelemy, A. Barrat, R. Pastor-Satorras, and A. Vespignani, *J. Theor. Biol.* **235**, 275 (2005).
  - [58] V. P. Zhdanov, *Surface Science Reports* **45**, 233 (2002).
  - [59] E. Panagakou, G. C. Boulougouris, and A. Provata, *Eur. Phys. J. B* **86**, 277 (2013).
  - [60] A. Provata, and E. Panagakou *submitted* (2014).
  - [61] O. E. Omel'chenko, M. Wolfrum, and Y. L. Maistrenko,

- Phys. Rev. E **81**, 065201(R) (2010).
- [62] G. C. Sethia, A. Sen, and F. M. Atay Phys. Rev. Lett. **100**, 144102 (2008).
- [63] Y. L. Maistrenko, A. Vasylenko, O. Sudakov, R. Levchenko, and V. L. Maistrenko (2014) arXiv:1402.1363v1.
- [64] I. Omelchenko, A. Provata, J. Hizanidis, E. Schöll, and P. Hövel, Phys. Rev. E **91**, 022917 (2015).
- [65] J. Feder, *Fractals*, Plenum Press, New York, 1988.

## Appendix A: Chimera states for connectivity matrices with gaps

Previous studies have demonstrated that the introduction of gaps in a system of coupled elements modifies the chimera states, producing different coherence-incoherence patterns [64]. We test this hypothesis in the case of the LLC model and investigate whether this effect is generic or exclusive to specific models. For this we consider an adjacency matrix,  $\{C_{kl}\}$ ,  $k, l = 1, \dots, N$ , with two gaps, one to the left and one to the right of the node  $k$ , around which the connectivity is described, called *reference node*. Generally, the size of the gaps and the sizes of the linked regions can vary independently on the left and on the right of the reference node. The form of matrix element  $C_{kl}$  is:

$$C_{kl} = \begin{cases} 1 & \text{if } k - R_3 < l < k + R_1 \\ & \text{or } k + R_1 + G_R < l < k + R_1 + G_R + R_2 \\ & \text{or } k - R_3 - G_L - R_4 < l < k - R_3 - G_L \\ 0 & \text{elsewhere,} \end{cases} \quad (\text{A1})$$

where all indices are taken modulo  $N$ . This general form indicates that the node  $k$  is linked to two groups of nodes to the right with sizes  $R_1$  and  $R_2$  which are separated by a gap of size  $G_R$ . A similar connectivity arrangement with linked groups of sizes  $R_3$  and  $R_4$  and gap size  $G_L$  applies to the left of each node. Symmetric connectivity is realized as a particular case of Eq. (A1) with  $R_3 = R_1$ ,  $G_L = G_R$  and  $R_4 = R_2$ . The connectivity matrix Eq. (A1), can be generalized further, to present multiple gaps to the left and to the right interrupting the linked elements. An asymmetric connectivity matrix, for instance, describes a directed network.

We now test the influence of the gap size using asymmetric connectivity matrices with links extending only to the right of each node. Because symmetry in the connectivity does not influence the relative fraction of nodes belonging to the (in)coherent part of the chimera, we only consider links to the right part of each node. This reduction is introduced to keep the number of parameters minimal; by using  $R_3 = R_4 = G_L = 0$  we only vary three parameters related to connectivity,  $R_1$ ,  $G_R$  and  $R_2$ .

To investigate the influence of the gap size on coherence, we keep the sizes of the two linked regions  $R_1$  and  $R_2$  constant, and vary only the gap size  $G_R$  in the interval  $0 \leq G_R \leq R_1 + R_2$ . In Fig. 10 we plot the typical chimera profiles as we increase the gap size  $G_R$ . The system size is kept to  $N = 1000$  oscillators, with parameter values  $p_1 = 300$ ,  $p_2 = 0.5$ ,  $p_3 = 0.8$ ,  $\sigma = 0.015$ . The total number of connections is also kept fixed,  $R = 400$ , and is divided into two regions  $R_1 = 100$  and  $R_2 = 300$ .

In Fig. 10 we observe changes in the chimera multiplicity, ranging from one to three (in)coherent regions, merging and splitting of coherent and incoherent regions and shifting of their position in space. The change of the chimera profiles can be quantified statistically by calculating the following measures of coherence [64]: a) the av-

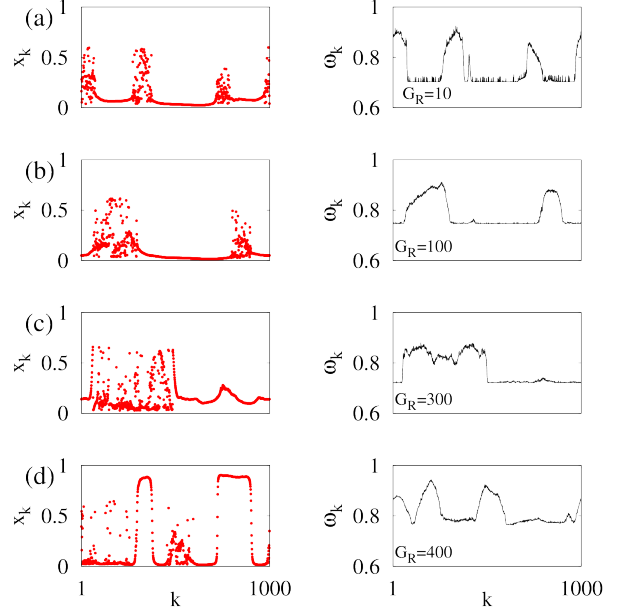


Figure 10: (Color online) Chimera states (left) and corresponding mean phase velocity profiles (right) for gap size variation. The gap sizes are indicated in the right panels, while  $R_1 = 100$  and  $R_2 = 300$ . All simulations start from the same initial conditions. Other parameters as in Fig. 2.

erage mean phase velocity of the coherent parts,  $\langle \omega_{\text{coh}} \rangle$ , b) the maximum difference of the mean phase velocities  $\Delta\omega = \omega_{\text{max}} - \omega_{\text{min}}$ , c) the fraction of oscillators belonging to the incoherent parts,  $N_{\text{incoh}}$ , and d) the extensive measure of incoherence  $M_{\text{incoh}}$ . The relative size  $N_{\text{incoh}}$  of the incoherent parts of the chimera state is calculated as:

$$N_{\text{incoh}} = \frac{1}{N} \sum_{k=1}^N \Theta(\omega_k - \langle \omega_{\text{coh}} \rangle - c) \quad (\text{A2})$$

where  $\Theta$  is the step function which takes the value 1 when its argument takes positive values and zero otherwise.  $c$  is a small tolerance, which in this case we set to 0.05. We also define the extensive, cumulative size  $M_{\text{incoh}}$  of the incoherent parts as:

$$M_{\text{incoh}} = \sum_{k=1}^N |(\omega_k - \langle \omega_{\text{coh}} \rangle)| \quad (\text{A3})$$

This is an extensive measure which represents the area below the arcs in the mean phase velocity profiles.  $M_{\text{incoh}}$  is a measure of incoherence and is equal to zero for fully coherent states.

In Fig. 11 the four coherence measures are plotted, averaged over 10 different initial conditions. Variation of the gap size shows a slight increase in the  $\omega_{\text{coh}}$  value for small values of  $G$ , which soon attains a constant value, independent of the gap size. The other three measures

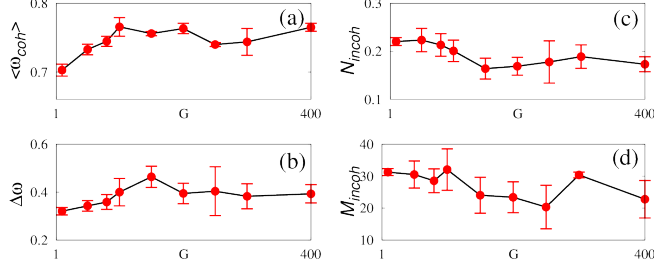


Figure 11: (Color online) The four measures of coherence as a function of the gap size  $G$ : a)  $\langle \omega_{coh} \rangle$ , b)  $\Delta\omega = \omega_{max} - \omega_{min}$ , c)  $N_{incoh}$ , d)  $M_{incoh}$ . Averages are taken over 10 different sets of initial conditions. Parameter values as in Fig. 10.

of coherence do not show any appreciable change with variations of the gap size. Especially the number of incoherent and coherent oscillators  $N_{incoh}$  and  $N - N_{incoh}$  do not change drastically with  $G$ , although the number of coherent and incoherent regions may change, as indicated by Fig. 10. This means that when the gap size changes there is a redistribution of the incoherent oscillators in

one large region (Fig. 10(c)) or in two or three smaller ones (Fig. 10(a),(b),(d)), so that the total number of incoherent oscillators is conserved (see Fig. 11).

Earlier studies for connectivity matrices with gaps in the FitzHugh-Nagumo system have demonstrated that the position of the gap is important and that it affects the chimera properties modifying all four measures of coherence [64]. To test this for the LLC model we produce the snapshots and corresponding mean phase velocity profiles varying the sizes of the connectivity regions  $R_1$  and  $R_2$  but keeping the total number of links  $R_1 + R_2 = 400$  fixed, while introducing a gap of constant size  $G_R = G = 100$  at various positions between the links. The results are depicted in Figure 12.

In contrast to the FitzHugh Nagumo system, here we do not observe a systematic dependence in the number of the (in)coherent regions as the gap of constant size moves away from the reference node. To further verify this, we plot in Fig. 13 the four measures of coherence for different values of  $R_1$ . Averages are taken over 10 different different initial conditions. All four measures seem to be constant (up to fluctuations) and they do not show any systematic change as a function of  $R_1$ .

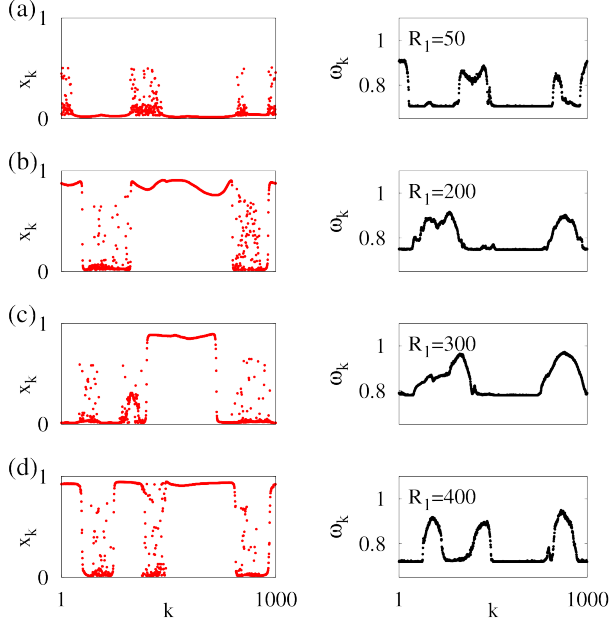


Figure 12: (Color online) Chimera states and corresponding mean phase velocity with variations on the position of a gap of constant size  $G_R = 100$ . (a)  $R_1 = 50, R_2 = 350$ , (b)  $R_1 = 200, R_2 = 200$ , (c)  $R_1 = 300, R_2 = 100$ , and d)  $R_1 = 400, R_2 = 0$ . All runs start from the same initial conditions. Other parameters as in Fig. 2.

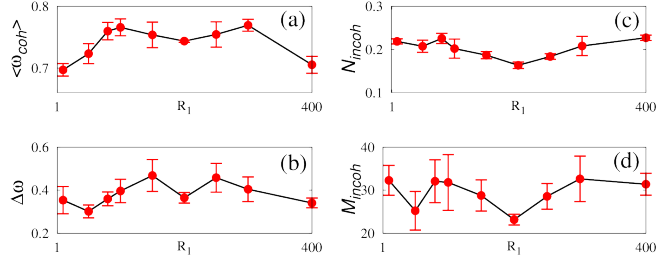


Figure 13: (Color online) The four measures of coherence as a function of the inner connectivity radius  $R_1$ , while  $R_1 + R_2 = 400$ : (a)  $\langle \omega_{coh} \rangle$ , (b)  $\Delta\omega = \omega_{max} - \omega_{min}$ , (c)  $N_{incoh}$ , (d)  $M_{incoh}$ . The gap size is kept to  $G_R = 100$ . Other parameter values as in Fig. 10. Averages are calculated over 10 different initial conditions.